JVI Journals.ASM.org

Structure of Crimean-Congo Hemorrhagic Fever Virus Nucleoprotein: Superhelical Homo-Oligomers and the Role of Caspase-3 Cleavage

Yi Wang,[a] Sujit Dutta,[b,c] Helen Karlberg,[d,e] Stéphanie Devignot,[f] Friedemann Weber,[f] Quan Hao,[a] Yee Joo Tan,[b,g] Ali Mirazimi,[d,e,h] and Masayo Kotaka[a]

Department of Physiology, Li Ka Shing Faculty of Medicine, University of Hong Kong, Pokfulam, Hong Kong SAR, China[a]; Institute of Molecular and Cell Biology, Agency for Science, Technology and Research (A*Star), Singapore[b]; School of Life Sciences and Chemical Technology, Ngee Ann Polytechnic, Singapore[c]; Center for Microbiological Preparedness/Swedish Institute for Infectious Disease Control, Solna, Sweden[d]; Department of Microbiology, Tumor and Cell Biology, Karolinska Institutet, Stockholm, Sweden[e]; Institute for Virology, Philipps University Marburg, Marburg, Germany[f]; Department of Microbiology, Yong Loo Lin School of Medicine, National University Health System, National University of Singapore, Singapore[g]; and Department of Clinical and Experimental Medicine, Linköping University, Linköping, Sweden[h]

Crimean-Congo hemorrhagic fever, a severe hemorrhagic disease found throughout Africa, Europe, and Asia, is caused by the tick-borne Crimean-Congo hemorrhagic fever virus (CCHFV). CCHFV is a negative-sense single-stranded RNA (ssRNA) virus belonging to the *Nairovirus* genus of the *Bunyaviridae* family. Its genome of three single-stranded RNA segments is encapsidated by the nucleocapsid protein (CCHFV N) to form the ribonucleoprotein complex. This ribonucleoprotein complex is required during replication and transcription of the viral genomic RNA. Here, we present the crystal structures of the CCHFV N in two distinct forms, an oligomeric form comprised of double antiparallel superhelices and a monomeric form. The head-to-tail interaction of the stalk region of one CCHFV N subunit with the base of the globular body of the adjacent subunit stabilizes the helical organization of the oligomeric form of CCHFV N. It also masks the conserved caspase-3 cleavage site present at the tip of the stalk region from host cell caspase-3 interaction and cleavage. By incubation with primer-length ssRNAs, we also obtained the crystal structure of CCHFV N in its monomeric form, which is similar to a recently published structure. The conformational change of CCHFV N upon deoligomerization results in the exposure of the caspase-3 cleavage site and subjects CCHFV N to caspase-3 cleavage. Mutations of this cleavage site inhibit cleavage by caspase-3 and result in enhanced viral polymerase activity. Thus, cleavage of CCHFV N by host cell caspase-3 appears to be crucial for controlling viral RNA synthesis and represents an important host defense mechanism against CCHFV infection.

The tick-borne Crimean-Congo hemorrhagic fever virus (CCHFV), a member of the *Nairovirus* genus of the *Bunyaviridae* family, is the causative agent of Crimean-Congo hemorrhagic fever (CCHF), a severe disease found throughout Africa, Europe, and Asia with a case fatality rate of up to 50% (26, 45, 46). The virus is transmitted to humans via infected tick bites or by direct contact with blood or tissue of viremic animals or humans. Clinical manifestations of CCHFV include sudden onset of fever, myalgia, headache, dizziness, sore eyes, photophobia, and hyperanemia. In severe cases, hemorrhagic manifestations develop several days after the onset of the disease (9, 46). Ribavirin, a nonimmunosuppressive nucleoside analogue with broad antiviral properties, is the only promising therapeutic agent against CCHFV, and there is no vaccine against this virus to date (11, 23, 25).

CCHFV is an enveloped virus with three negative-sense single-stranded RNA (ssRNA) genomes named S, M, and L encoding the nucleoprotein (N), glycoproteins Gn and Gc, and the RNA-dependent RNA polymerase (RdRp) (L), respectively (27, 42, 43). CCHFV N is significantly larger than Ns from other genera from the *Bunyaviridae* family (7). Similarly to other negative-sense RNA viruses, the CCHFV RNA genome is encapsidated by CCHFV N to form the ribonucleoprotein (RNP) complexes. Encapsidation of the CCHFV genomic RNA is essential in the replicative cycle and the packaging of the genome into the virions; however, little is known about the mechanism of interaction of CCHFV N with the genome RNA and the formation of RNPs (27). Studies of other bunyaviruses revealed that specificity in RNA recognition by Ns differs from genus to genus. While some are specific in the identification of RNA sequence, others bind non-specifically to the ssRNAs (30, 34, 38). The recent structural determination of N of Rift Valley fever virus (RVFV), a member of the *Phlebovirus* genus, showed weak binding affinity of N with ssRNA. In addition, a conformational change in the protein is implicated during oligomerization to form the RNP complex (10, 33).

During the preparation and review of the manuscript, structures of the CCHFV N monomer of strain YL040570 and strain Baghdad-12 were published (6, 14). The study by Guo et al. showed that the CCHFV N monomer has weak RNA-binding affinity and has distinct metal-dependent DNA-endonuclease activity (14). The study by Carter et al. revealed a different conformation adopted by CCHFV N with a transposition of the arm domain and revealed surfaces likely to be involved in RNA binding and oligomerization (6). In the present study, we have determined the structure of CCHFV N in two different conformations: one resembling the oligomerized RNP form and the other being the free monomeric form. We have previously identified the presence of a

Received 28 June 2012 **Accepted** 28 August 2012
Published ahead of print 5 September 2012
Address correspondence to Masayo Kotaka, masayo@hku.hk, or Ali Mirazimi, ali.mirazimi@smi.se.
Y. Wang and S. Dutta contributed equally to this work.
Supplemental material for this article may be found at http://jvi.asm.org/.

doi:10.1128/JVI.01627-12

conserved caspase-3 proteolytic cleavage site in CCHFV N by analyzing its primary sequence. We have also demonstrated that during CCHFV infection, host cell caspase-3 activation results in the cleavage of CCHFV N into a 30-kDa fragment, suggesting that caspase-3-dependent cleavage of CCHFV N may represent a host cell defense mechanism against CCHFV infection (21). Our structures revealed that a conformational change has to occur to convert CCHFV N from the oligomerized form to the free monomeric form. Only when CCHFV N is in its free monomeric form would the caspase-3 cleavage site be exposed for host cell caspase-3 cleavage. Mutations at the caspase-3 cleavage site abolishing caspase-3 cleavage of CCHFV N would result in enhancement of CCHFV polymerase activity during viral RNA (vRNA) transcription.

MATERIALS AND METHODS

Cloning, expression, and purification. A cDNA encoding a fragment of CCHFV N was inserted into a pGEX6P1 vector (GE Healthcare) with a glutathione *S*-transferase (GST) tag fused to the N terminus of the protein. The resulting clone was transformed into *Escherichia coli* BL21 Codon$^+$ RIL (DE3) cells (Stratagene). To induce protein expression, isopropyl-D-1-thiogalactopyranoside (IPTG) was added to a final concentration of 0.2 mM when the optical density at 600 nm (OD_{600}) of the bacterial culture reached 0.6, and the culture was grown for another 20 h at 16°C. Cells were harvested by centrifugation and resuspended in lysis buffer (50 mM Tris-HCl, pH 7.4, 500 mM NaCl, 2 mM dithiothreitol [DTT], 0.1 mM phenylmethylsulfonyl fluoride [PMSF]). The resuspended cells were sonicated on ice and cleared by centrifugation.

The cleared cell lysate was loaded onto a glutathione Sepharose 4 Fast Flow column (GE Healthcare) preequilibrated with the lysis buffer. The column was then washed with 50 ml of lysis buffer containing 1 M NaCl. After a final wash with 30 ml of lysis buffer, on-column cleavage with 1.5 mg PreScission protease (GE Healthcare) to release CCHFV N from the GST tag was performed with incubation at 4°C overnight. Cleaved CCHFV N was collected, concentrated, and subjected to size exclusion chromatography using a Superdex 200 16/60 column (GE Healthcare) preequilibrated with 50 mM Tris-HCl, pH 7.4, 2 mM DTT. As a final polishing step, the fractions containing CCHFV N were pooled and loaded onto a cation exchange HiTrap SP column (GE Healthcare) preequilibrated with 50 mM Tris-HCl, pH 7.4, 2 mM DTT and eluted by a linear gradient of 0 to 1 M NaCl buffer. At each step in the purification procedure, fractions were analyzed by SDS-PAGE and appropriate fractions were pooled. The eluted protein was concentrated to 10 mg/ml, flash frozen, and stored at −80°C until further use.

Preparation of SeMet-incorporated CCHFV N. The plasmid coding for N-terminally GST-tagged CCHFV N was transformed into the B834(DE3) Met$^-$ strain for expression of selenomethionine (SeMet)-incorporated CCHFV N using standard protocols (17). Briefly, an overnight culture of transformed cells was inoculated into LB supplemented with ampicillin and incubated at 37°C. The cells were harvested when the OD_{600} reached 0.2 and washed twice in SeMet base medium (Molecular Dimensions). The washed cells were then used to inoculate prewarmed Athena minimal medium supplemented with nutrient mix (Molecular Dimensions), 40 μg/ml selenomethionine (Calbiochem), and ampicillin to a final OD_{600} of 0.02. The culture was incubated at 37°C until the OD_{600} reached 0.5. At this point, the culture was induced with IPTG and the expression assay was carried out at 16°C overnight. SeMet CCHFV N was purified according to the same procedures as those for native CCHFV N. The purity of SeMet-incorporated CCHFV N determined by SDS-PAGE analysis is >99%. The eluted protein was concentrated to 8 mg/ml, flash frozen, and stored at −80°C until further use.

Crystallization. Screening of crystallization conditions was performed using Mosquito liquid handler (TTP Labtech) at 291 K using the sitting-drop vapor diffusion method by mixing 100 nl protein with an equal volume of crystallization solution. Of the 576 conditions screened, initial hits for native apo-CCHFV N were observed under PEGs suite (Qiagen) condition 7 (0.1 M morpholineethanesulfonic acid [MES], pH 6.5, 40% [vol/vol] polyethylene glycol [PEG] 200). After optimization, the best crystals of native apo-CCHFV N grew in 0.1 M MES, pH 6.5, 37% (vol/vol) PEG 200, 12% (vol/vol) PEG 400. SeMet-incorporated CCHFV N crystals grew under the same conditions as did native apo-CCHFV N.

For poly$(U)_{12}$ ssRNA-incubated CCHFV N, 6 mg/ml of CCHFV N was mixed with 10 μM RNA and crystals were grown in 0.1 M MES, pH 6.5, 12% (vol/vol) PEG 500 by using sitting-drop vapor diffusion.

Data collection, selenium MAD phasing, and model refinement. Crystals of both the wild-type and SeMet-labeled apo-CCHFV N were serially transferred into the cryoprotectant, which was a mixture of 20% and 30% PEG 400 with the reservoir solution described above (five steps of soaking, 2 min per step, 291 K). As for poly$(U)_{12}$ ssRNA-incubated CCHFV N, a mixture of 30% PEG 100 as well as 5% ethanol with the reservoir solution served as the cryoprotectant. Data were collected at beamline 13B1, NSRRC, Taiwan, for both native and SeMet-labeled apo-CCHFV N crystals frozen and maintained at 100 K. A fluorescence scan was used to set the optimal peak wavelength for the selenium edge. Data collection statistics of native and SeMet-labeled CCHFV N crystals are shown in Table 1. Data were indexed and integrated with HKL2000 (31). The SHELX suite (36) was used to calculate phases from the selenium multiwavelength anomalous diffraction (MAD) data (data set 2 in Table 1). Following data preparation with SHELXC, SHELXD identified a total of 39 selenium sites. Electron density maps calculated with SHELXE without further density modification were interpretable. Automated model building was carried out with PHENIX (42), and the rest of the model was built manually with COOT (8) and O (20). The structure was refined in CNS (4), using simulated annealing and B-factor refinement, and Refmac5 (47). The partially refined structure from the MAD data was used to solve the higher-resolution native data by molecular replacement, which was refined in CNS and Refmac5, as described above.

The program PHASER (26) was used to solve the structure of poly$(U)_{12}$ ssRNA-incubated CCHFV N by molecular replacement. The body and stalk regions of one molecule of apo-CCHFV N were used as two separate ensembles for the rotational and translational search. The resulting structure was refined in CNS (4), using simulated annealing and B-factor refinement. Refinement statistics for apo-CCHFV N and poly$(U)_{12}$-incubated CCHFV N are shown in Table 1.

CCHFV N mutants and minireplicon assay. PCR methods were used to generate substitution mutants of CCHFV N, where the aspartic acid residues at positions 266 and 269 in the primary sequence were changed to alanine. Mutated sequences were ligated into the 5′ BamHI and 3′ XhoI site of PXJ40 expression plasmid. DNA sequence analysis was carried out to confirm amino acid substitutions.

Functional analysis of N constructs was conducted using the CCHFV minireplicon system developed by Bergeron et al. (3). BSR T7/5 cells were grown in Dulbecco's modified Eagle's medium (Life Technologies), supplemented with 10% newborn calf serum (Life Technologies), 5% tryptose phosphate broth (Sigma-Aldrich), 1% nonessential amino acids (Life Technologies), 1% L-glutamine (Life Technologies), 1% penicillin-streptomycin (Life Technologies), and freshly added 2% Geneticin (Life Technologies). Subconfluent BSR T7/5 cells were transfected with jetPRIME transfection reagent (Polyplus transfection) with a mix of plasmids: 600 ng of wild-type or inactive CCHFV RdRp (pCAGGS_L_wt or pCAGGS_L_ΔDD), 200 ng of wild-type or mutated CCHFV N (pXJmyc_N_blast or pXJmyc_N_D266 + 269A), 200 ng of minigenome [V(0.0)_vS_Gluc(1G)], 200 ng of T7 polymerase (pCAGGS_T7), and 100 ng of constitutively expressed firefly luciferase transfection control (pGL3-luc). Four hours after transfection, the transfection medium was replaced with fresh medium. Cell supernatants were collected 48 h posttransfection, and *Gaussia* and firefly luciferase activities were measured in cell lysates by the dual-luciferase reporter assay system (Promega) according to the manufacturer's protocol, using a Centro LB 960 microplate luminometer (Berthold Technologies). Student's *t* test was used for cal-

TABLE 1 Data collection, phasing, and refinement statistics for CCHFV N

Statistic	Native Apo, data set 1	SeMet-incorporated Apo, data set 2	Native Apo incubated with 12-U RNA
Data collection			
Space group	$P3_121$	$P3_121$	$P2_12_12_1$
a, *b*, *c* (Å)	133.11, 133.11, 289.14	133.78, 133.78, 291.19	52.78, 64.50, 127.72
α, β, γ (°)	90, 90, 120	90, 90, 120	90, 90, 90
Wavelength	1.0	0.978/0.963[c]	1.0
Resolution (Å)	30–3.10 (3.21–3.10)	30–3.55 (3.68–3.55)/30–3.50 (3.60–3.50)[c]	30–2.80 (2.90–2.80)
R_{sym}[a]	0.075 (0.875)	0.129 (0.906)/0.132 (0.978)[c]	0.134 (0.775)
$I/\sigma I$	20.6 (1.6)	14.3 (1.2)/13.9 (1.2)[c]	17.0 (1.4)
Completeness (%)	99.9 (100)	98.7 (89.0)/99.2 (93.3)[c]	99.7 (96.8)
Redundancy	5.5 (5.6)	5.2 (3.8)/5.3 (4.0)[c]	12.9 (7.9)
Wilson B-factor	111.3		73.2
No. of molecules/ASU[d]	3		1
Refinement			
Resolution		30–3.10	30–2.80
No. of reflections		49,003/2,769	10,663/533
R_{work}/R_{free}		0.170/0.233	0.199/0.244
No. of atoms			
Protein		11,088	3,659
Ligand/ion		20	5
Water		289	41
B-factors			
Protein		95.3	71.7
Ligand/ion		122.9	95.0
Water		66.0	51.2
RMSD			
Bond lengths (Å)		0.011	0.009
Bond angles (°)		1.39	1.44
Ramachandran plot[b]			
% most favored		93.9	92.3
% additionally allowed		5.9	7.4
% generously allowed		0.1	0.2
% disallowed (residue no.)		0.1 (A152)	0

[a] Highest-resolution shell is shown in parentheses.
[b] As defined by PROCHECK (22).
[c] Values are shown as inflection/remote.
[d] ASU, asymmetric unit.

culation of significant differences between wild-type and DEVD mutant N in the minireplicon assay. A *P* value of <0.05 was considered significant.

***In vitro* caspase-3 cleavage assay.** The purified CCHFV N (2 mg/ml) was incubated with or without 100 μM poly(U)$_{12}$ ssRNA (Lifetech) for 48 h at 4°C. The mock- or poly(U)$_{12}$ ssRNA-treated CCHFV N was treated with caspase-3 (Biovision) according to the manufacturer's protocol.

SDS-PAGE and Western blot analysis. Samples from the *in vitro* caspase-3 cleavage assay were resuspended in reducing sample buffer (10 mM Tris-HCl, 0.5% SDS, 10% glycerol, 2% β-mercaptoethanol), boiled for 5 min, and separated by SDS-PAGE using precast gels from Lifetech. When supernatants were collected separately, the supernatant was centrifuged and resuspended and handled as described above. Electrophoresis was carried out at 200 V, and proteins were transferred to nitrocellulose membranes using a transfer buffer containing 25 mM Tris, 192 mM glycine, and 20% methanol at 100 V for 1 h. Membranes were blocked in 5% nonfat dried milk overnight at +4°C. After being washed in phosphate-buffered saline (PBS) containing 0.01% Tween (PBST), the membranes were incubated with a mouse monoclonal anti-CCHFV N (monoclonal antibody [MAb] CCHFV N) antibody for 1 h at room temperature and then washed with PBST before addition of goat anti-mouse horseradish peroxidase (HRP)-conjugated antibody (Bio-Rad). After incubation at room temperature for 1 h, the membranes were washed in PBST. Proteins were detected with ECL Plus Western blotting detection reagents (GE Healthcare) according to the manufacturer's protocol. All antibodies were diluted in blocking buffer in PBS containing 0.2% bovine serum albumin (BSA) and 0.1% Triton X-100.

Protein structure accession numbers. The coordinates and structural factors of the structures were deposited in the Protein Data Bank (PDB) under PDB codes 4AQF and 4AQG for the oligomeric and monomeric forms of CCHFV N, respectively.

RESULTS

Recombinant CCHFV N forms RNA-binding oligomers. Recombinant CCHFV N from strain IbAr10200 (2, 12, 39) was overexpressed in *E. coli* with an N-terminal cleavable GST tag and purified. Size exclusion chromatography of cleaved CCHFV N revealed two peaks, P1 and P2 (see Fig. S1 in the supplemental material). SDS-PAGE analysis revealed that both peaks contained a protein with a size consistent with that of CCHFV N (55 kDa), indicating that CCHFV N was the only protein present. The position of peak P1 corresponds to a protein species with an apparent molecular mass of over 300 kDa, suggesting the presence of higher-order oligomeric states of CCHFV N. The position of peak P2 corresponds to an apparent molecular mass of ~60 kDa, sug-

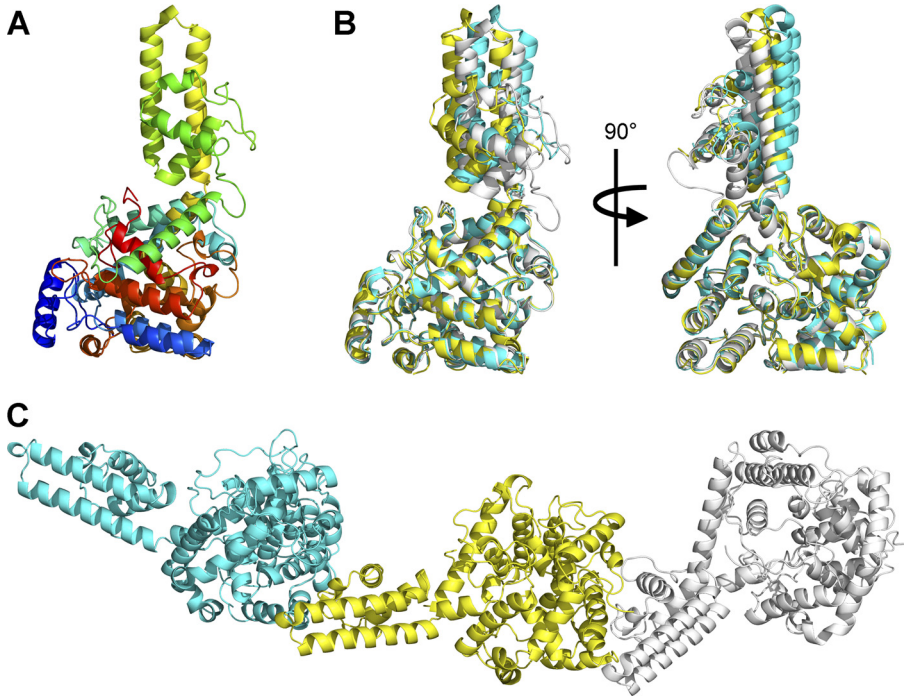

FIG 1 (A) Crystal structure of CCHFV N. The structure is colored in rainbow colors from blue at the N terminus to red at the C terminus. (B) Superposition of 3 molecules of CCHFV N shows differences in the degree of bend of the stalk region. The three molecules, namely, A, B, and C, of CCHFV N in the asymmetric unit are colored in yellow, white, and cyan, respectively. (C) Head-to-tail oligomerization of the 3 molecules of CCHFV N in the asymmetric unit. The color scheme is the same as that in panel B.

gesting the presence of monomeric CCHFV N species. Measurement of the OD_{260}/OD_{280} ratio for P1 and P2 was performed to test for the presence of bound nucleic acids. The higher-order CCHFV N oligomer (P1) coeluted with nucleic acids, presumably RNA from *E. coli*, with a ratio of 1.49, while peak P2, with a ratio of 0.69, is devoid of bound nucleic acids (18).

Crystal structure of CCHFV N in an oligomerized form. Using the P2 peak devoid of nucleic acids, recombinant CCHFV N was crystallized and the structure was solved by two-wavelength anomalous diffraction from the selenomethionine (SeMet)-incorporated CCHFV N to 3.3-Å resolution and extended to 3.1-Å resolution for the native protein (Table 1). In this crystal form, there are 3 CCHFV N molecules per asymmetric unit of the space group $P3_121$. The crystal structure reveals that the CCHFV N molecules consist of an orthogonal bundle of 21 α-helices and can be divided into the globular body and stalk domains. The N-terminal domain of residues 1 to 183 (α1 to α9) and C-terminal domain containing residues 295 to 482 (α14 to α21) combine to form the globular body, while the central domain (residues 195 to 294, α10 to α13) forms a stalk protruding from the globular body (Fig. 1A). The three molecules of CCHFV N in the asymmetric unit are nearly identical in conformation, with an overall root mean square deviation (RMSD) of 1.490 to 1.853 Å.

Of the three molecules of CCHFV N in the asymmetric unit, we were able to observe clear electron density only of the flexible linker residues 181 to 195 connecting the stalk domain and the globular body domain in molecule B (see Fig. S2 in the supplemental material). The linker is not visible in molecules B and C, and unobserved disordered residues include 181 to 194 in molecule A and 181 to 195 in molecule C. The intrinsic flexibility for this linker region is required to allow for the conformation change observed and discussed below.

The overall architecture of our CCHFV N structure of strain IbAr10200 with a globular body and protruding stalk is similar to that of the recently published CCHFV N structure of strain YL040570 (14), which has a 97% amino acid sequence identity to our CCHFV N (see Fig. S3A in the supplemental material). Similarly, a Dali search with our CCHFV N structure revealed that the globular body of our CCHFV N is similar to the N-terminal nucleotide-binding domain of Lassa virus nucleoprotein (LASV N) (5, 16, 32) (RMSD for 251 equivalent Cαs of 4.4 Å, Z score = 13.1, for the A chain of PDB entry 3WMP [16]). Surface rendering of the globular body revealed a deep basic cavity channeling between the head and body regions similar to the cap-RNA/RNA-binding crevice found in the N-terminal domain of LASV N (16). When the head domains of all three CCHFV N molecules of the crystallographic asymmetric unit were superposed on one another, they exhibited an average RMSD of ~0.63 Å, indicating that little conformational change had occurred. Attempts to cocrystallize or soak cap-nucleotide analogues and short ssRNAs of 3 to 5 bases in length proved unsuccessful, as they resulted in crystals growing in the same crystal form as the apo structure with no extra electron density resembling bound nucleotides or RNA observed in this potential nucleotide-binding site.

The stalk domain protrudes from within the head domain and is an alpha-helical bundle composed of the central residues 191 to 294 (α10 to α13) with the two longest α-helices, α12 and α13, forming the antiparallel arm extending from the body. The stalk domains of the three molecules of CCHFV N in the asymmetric unit are nearly identical, with an average RMSD of ~0.50 Å. The

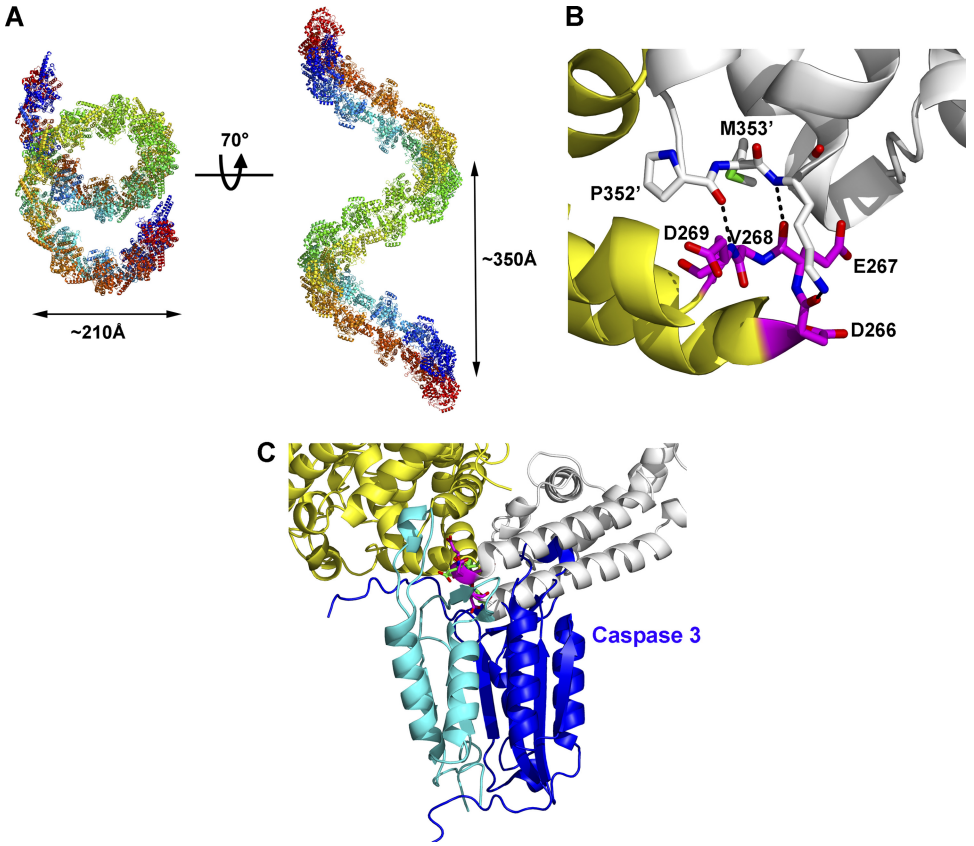

FIG 2 (A) Antiparallel double superhelix polymer of CCHFV N. Each superhelix is colored in rainbow colors from blue to red. (B) Head-to-tail interactions of CCHFV N molecules at the caspase-3 cleavage site. One CCHFV N molecule is colored white. The adjacent CCHFV N involved in the head-to-tail interaction is colored yellow, with its residues that are identified as the caspase-3 cleavage site colored in magenta. (C) The caspase-3 cleavage site is obscured in the superhelical polymer. The caspase-3 cleavage site of CCHFV N in the superhelical form was superposed onto the structure of the inhibitor peptide bound to caspase-3 (PDB accession code 2CJX). The color scheme for CCHFV N is the same as that in panel B. The caspase-3 heterodimer is colored in cyan and blue, and the bound inhibitor peptide is colored in green.

positions of the stalk domains of the three CCHFV N molecules with respect to their globular body domains are slightly different, as revealed by superposition of the body domains (Fig. 1B).

As mentioned previously, the overall architecture of our CCHFV N structure is similar to that of the recently published structure of strain YL040570 (14). When the molecules of our crystal structure were superposed onto that of the published structure, an average RMSD of ~9.15 Å was observed for all equivalent Cαs, indicating a difference in overall conformation. Superposition of the globular bodies and the stalk domains separately resulted in an average RMSD of 0.914 Å and 1.691 Å, respectively, for all equivalent Cαs. Apart from differences in sequence between the two strains, close examination revealed that, while the globular bodies of our CCHFV N molecules are virtually identical to that of the reported structure, slight discrepancies are observed in the stalk region. In particular, a one-amino-acid displacement is observed in the region flanking α11, from R225 to K244 (see Fig. S3B in the supplemental material), where in the published structure of strain YL040570, waters were built in place of longer side chains of the displaced amino acids where clear density is shown. In addition, the positions of the stalk domains are very different in the two structures (see Fig. S3C).

Oligomerization of CCHFV N. In this crystal form, the three CCHFV N molecules in the asymmetric unit are organized in a head-to-tail manner with the stalk of one molecule interacting with the base of the globular body of the adjacent molecule (Fig. 1C), and this interaction is repeated in a directional manner along the $P3_1$ screw axis. In addition, along the crystallographic 2-fold axis, the CCHFV N molecules interact with the symmetry-related molecules to form antiparallel head-to-tail dimers. Together, CCHFV N molecules are seen to form an antiparallel double superhelix of nine molecules per turn per helix of about 210 Å in diameter and about 350-Å rise, running through the crystal along the crystallographic *c* axis (Fig. 2A). Crystallization of monomeric N protein in solution into an oligomerized form is not uncommon; it has been previously demonstrated that the monomeric N protein of RVFV is also able to crystallize to form hexameric rings (10). While in solution, the stabilization of the oligomers may require the presence of RNA-bound subunits; the high CCHFV N protein concentration in crystallization trials may drive the N proteins to form larger stable oligomers.

Oligomerization of CCHFV N along one helix is driven by the interaction of the stalk with the base of the globular body of the adjacent CCHFV N. Although the contacts are slightly different due to the difference in the degree of bending of the stalk domain as discussed above, all stalk-body interactions involve extensive hydrogen bonds and van der Waals contacts between residues 320 to 354 of α16-α17 at the base of the body domain of one molecule

and residues 210 to 219 and 260 to 272 of the α12-α13 loop in the stalk region of the adjacent molecule. In particular, main chain interactions are observed between residues 352 to 354 of the α17-α18 loop of the body domain and residues 266 to 269 at the α12-α13 loop in the stalk region of the adjacent molecule (Fig. 2B), which was previously identified as the caspase-3 cleavage site (14, 21).

Turning to the dimerization interfaces along the double superhelix, the two molecules of the dimer are related by crystallographic 2-fold symmetry, with helices α2, α3, and α6 stacking to their antiparallel equivalents; the buried surface areas of the antiparallel head-to-tail dimers are calculated to be between 1,171.9 and 1,772.9 Å^2, constituting 5.7% to 8% of the total surface area of a CCHFV N molecule, and are located at the body-stalk boundary of CCHFV N. Major contacts seen at the dimer interface involve the interaction of the antiparallel globular bodies with the α7-α8 loop stacked against its antiparallel equivalent and α9 of one molecule interacting with the α20-α21 loop of its counterpart. The difference in buried surface areas observed is due to the difference in the degree of bending of the stalk region observed in the three molecules. In addition, the existence of differently bent conformations of the stalk demonstrates the ability of CCHFV N to form superhelices with different molecular organizations and thus provides a basis for the formation of supercoiled, string-like RNP structures.

Viral genomic RNA binding. Analysis of the electrostatic surface potential of the CCHFV N molecule revealed two other positively charged regions apart from the positively charged crevice identified in the globular body reminiscent of the RNA-binding crevice of LASV N. The first region is found on the globular body constituted by K132, R134, K135, and N468 (Fig. 3A). The other large positively charged region is found at the stalk region, composed of residues H197, K222, R225, K282, K286, and K292 (Fig. 3A). The basic residues identified in these two regions are well conserved in the Ns across the *Nairovirus* genus (see Fig. S5 in the supplemental material) and thus suggest a role in RNA binding. Furthermore, analysis of the electrostatic surface potential of part of the CCHFV N double superhelix reveals a positively charged crevice located on the outside of the double helix (Fig. 3B). This stretch of positively charged residues extends from the positively charged patch comprising residues R134 and N468 on the globular body to the equivalent positively charged patch on the juxtaposed antiparallel CCHFV N molecule via the positively charged crevice contributed by the positively charged region composed of residues H197, K222, R225, K282, K286, and K292 of the stalks and residues K342, K343, and K346 at the base of the neighboring globular body, at the dimer interface of the antiparallel superhelices. The presence of sulfate ions bound to the crevice at the dimer interface in our structure supports the notion that this positively charged crevice on the outside of the double superhelix may serve as an RNA-binding cleft.

The caspase-3 cleavage site is involved in oligomerization of CCHFV N. We have previously demonstrated that during CCHFV infection, host cell caspase-3 activity is induced and CCHFV N is cleaved at the conserved proteolytic cleavage site DEVD into a 30-kDa fragment. Mutations of D226 and D229 to alanine would abolish cleavage of CCHFV N by host cell caspase-3 (21). Interestingly, this previously identified conserved caspase-3 cleavage site is found to be located at the α12-α13 loop of the stalk domain and is directly involved in the head-to-tail interaction of the CCHFV N molecules in the formation of the superhelical oligomeric form of CCHFV N as discussed above (Fig. 2A). Modeling of interaction with caspase-3 at the caspase cleavage site of CCHFV N in this superhelical form reveals that the head-to-tail interaction of CCHFV N molecules obscures the caspase-3 cleavage site and thus would prevent binding and subsequent cleavage by caspase-3 (Fig. 2C).

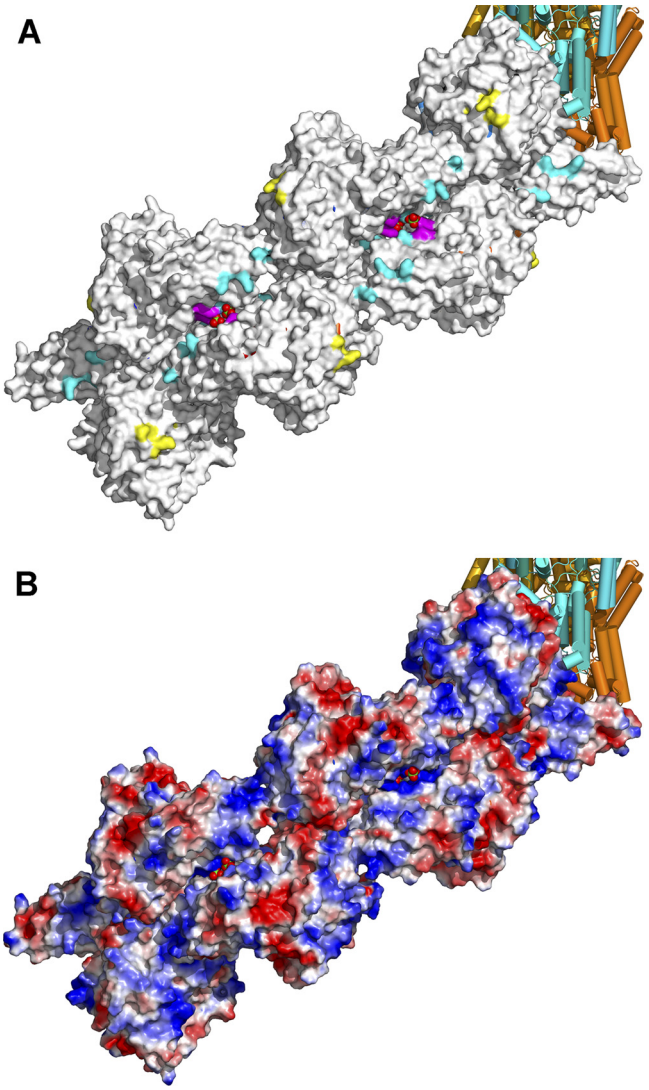

FIG 3 Possible RNA-binding site of CCHFV N superhelical polymer. (A) Conserved clusters of positively charged residues that were identified are shown for part of the CCHFV N double superhelix. Yellow, cyan, and magenta surfaces depict the clusters composed of residues K132, R134, K135, and N468; residues H197, K222, R225, K282, K286, and K292; and residues K342, K343, and K346, respectively. (B) Electrostatic surface potential of the same part of the CCFHV-N double superhelix. Sulfate ions in the positively charged crevice are shown in spheres.

Incubation with primer-length ssRNA results in conformational change of CCHFV N and release of monomeric CCHFV N. In the attempt to identify the possible RNA-binding sites of CCHFV N in the superhelical form, we performed cocrystallization of CCHFV N with ssRNAs of different lengths. As previously discussed, cocrystallization of CCHFV N with short, 3- to 5-base ssRNAs yielded the same crystal form as that with the apo-CCHFV

N without additional electron density resembling bound RNA. We therefore decided to increase the length of the ssRNA used and utilized primer-length 12- to 16-base-long ssRNAs to perform cocrystallization. Unexpectedly, when CCHFV N was crystallized in the presence of primer-length ssRNAs, it crystallized under a different condition in a different space group with different unit cell dimensions, and only one CCHFV N molecule is observed in the asymmetric unit (Table 1). When the structure of CCHFV N in this conformation was superposed with the published structure of CCHFV N of strain YL040570 (14), an overall RMSD of 1.6 Å of all equivalent Cαs was observed, indicating that CCHFV N in this conformation is similar to that of the published structure. Again, the major discrepancy is the one-amino-acid displacement in the region flanking α11, from R225 to K244 of the stalk (see Fig. S3B in the supplemental material). No electron density was observed for any bound RNA. Analysis using analytical size exclusion chromatography revealed, upon incubation with primer-length ssRNAs, an additional peak with a migration size of a position corresponding to ~40 kDa. SDS-PAGE analysis of the peak fractions revealed this peak to be CCHFV N with no degradation (see Fig. S4). The OD_{260}/OD_{280} ratio of 0.507 for the peak revealed that there was no primer-length ssRNA bound to the CCHFV N of this peak. The change in migration size upon incubation with primer-length ssRNAs indicated that a conformational change of CCHFV N has occurred without binding of ssRNA, thereby affecting the migration pattern on the size exclusion column.

Superposition of the monomeric CCHFV N structure on the molecules from the superhelical structure revealed that a conformational change indeed had occurred upon incubation with primer-length ssRNAs. The key changes included the winding up of α13 and α14 into a long α-helix at the hinge S294, resulting in the rotation of the stalk domain by ~168° (Fig. 4A and B). Upon rotation of the stalk domain, the head-to-tail interaction of the CCHFV N molecules in the superhelical structure via the α12-α13 loop at the tip of the stalk becomes disrupted. In addition, the rotation of the stalk domain would cause steric hindrance at the dimer interface of the antiparallel helical structure, resulting in the disruption of the dimeric interactions (Fig. 4C). As a result, monomeric CCHFV N will be released from the ends of the double superhelical CCHFV N polymer. This release of the free, monomeric N would result in the exposure of the caspase-3 cleavage site situated at the loop region at the tip of the stalk domain to host cell caspase-3. To confirm this hypothesis, we incubated purified recombinant N with or without ssRNA followed by treatment with human caspase-3. Indeed, enhanced cleavage of CCHFV N by caspase-3, resulting in the release of the 30-kDa cleavage product, is observed only in the presence of primer-length ssRNA (Fig. 4D and E). This corroborates our observation from the crystal structures whereby the presence of primer-length ssRNA would cause the exposure of the caspase-3 cleavage site of CCHFV N by inducing a conformational change in CCHFV N.

Mutation of the CCHFV N caspase-3 cleavage site enhances viral RNA synthesis. CCHFV N is an important component in the viral transcription and replication machinery. In order to determine the effect of the caspase-3 cleavage site of CCHFV N on viral RNA synthesis activity, minireplicon assays were performed using wild-type CCHFV N or a CCHFV N mutant with the conserved cleavage site mutated to evade caspase-3 cleavage. The results, with a *P* value of 0.027, demonstrated that by abolishing the caspase-3 cleavage site of CCHFV N, RNA synthesis by CCHFV polymerase is enhanced (Fig. 5). Enhanced minireplicon expression of the mutant N also implied that the mutations did not affect the oligomerization of CCHFV N to form the superhelical RNP structure, as the interaction between the DEVD loop and the globular body is mainly via main chain interactions rather than side chain interactions. Attempts were made to detect cleaved wild-type CCHFV N fragments by Western blotting; however, no cleavage products were detected, presumably because concentrations of cleaved N from the minireplicon assay were below detectable levels. Although we cannot exclude the possibility that mutations of the caspase-3 cleavage site in CCHFV N affect viral RNA synthesis in other ways, such as changing the dynamics of conformational change from superhelical oligomers to free monomeric form and vice versa, the results of the minireplicon assay are consistent with our previous data showing that titers of CCHFV can be increased by caspase-3 inhibition (21).

DISCUSSION

CCHFV N is the most abundant viral protein in the CCHFV particles, playing a key role in the encapsidation of viral genomic and antigenomic RNAs. Nucleoprotein structures of other segmented and nonsegmented RNA viruses have been determined in the absence and presence of RNA (1, 5, 10, 13, 15, 16, 32, 33, 41, 48). Here, we have determined the crystal structure of CCHFV N in a double superhelical oligomeric form and a monomeric form. The double superhelical structure of CCHFV N presented in this report is in a relaxed helical state and could represent the physiological organization of CCHFV RNP, as previous studies have revealed that, unlike nucleocapsids of nonsegmented viruses, which are tightly packed rigid helical structures (24), nucleocapsids of bunyaviruses and arenaviruses are more relaxed and form irregularly shaped RNPs (24, 29, 33, 35, 37). The bending of the stalk domain in CCHFV N appears to be crucial for the oligomerization of CCHFV N, as it mediates the interaction with the adjacent molecule in the superhelical structure and allows dimerization of the superhelices to form an antiparallel double super helix. Moreover, the flexibility in the degree of bend by the stalk region in its oligomerized state would allow CCHFV N to organize into RNP structures of different morphologies, as observed in previous electron microscopy (EM) studies for bunyaviruses (33).

Unexpectedly, we observed a conformational change of CCHFV N when it was incubated with primer-length ssRNAs of 12 to 16 U's. This conformational change is anticipated to disrupt the double superhelical CCHFV N polymer, causing it to release monomeric CCHFV N. The conformational change of CCHFV N after treatment with primer-length ssRNA suggests a possible model for how replication and transcription of CCHFV viral RNA (vRNA) would occur. In this model, the double superhelical CCHFV N polymer would represent the RNP with vRNA bound to the positively charged crevice on the outer periphery of the polymer. When vRNA is bound to the CCHFV N polymer, the bound portion of RNA would be protected by CCHFV N and would not be available to form duplexes. During transcription and replication, CCHFV, like other members of the *Bunyaviridae* family, utilizes a short capped RNA fragment of 10 to 20 nucleotides (nt) in length snatched from host cell mRNAs to initiate RNA synthesis (19). From our results, it appears that the presentation of these RNA primer fragments by the CCHFV N superhelical polymer would trigger a conformational change of the subunits, causing the stalk domain to rotate away from its position in the double

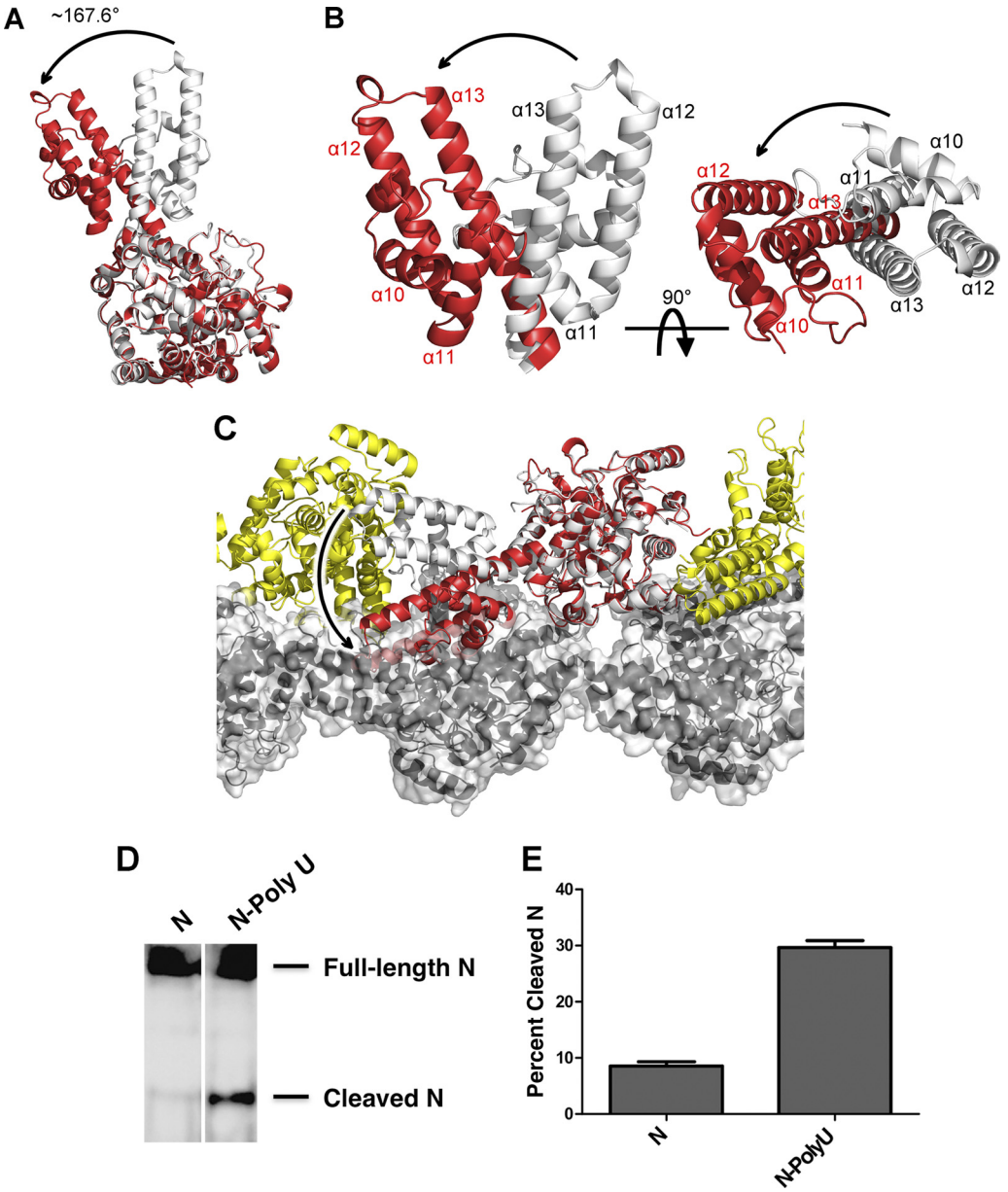

FIG 4 Conformational change of CCHFV N upon incubation with primer-length RNA. (A) Rotation of the stalk region upon incubation with primer-length RNA. The CCFHV N molecule in superhelical form is shown in white, and that in monomeric form is shown in red. (B) Conformational changes in the stalk domain. The color scheme is the same as that in panel A; only the stalk domains are shown for clarity. The arrow indicates the direction of movement. (C) Disruption of oligomerization by the conformational change. The color scheme is the same as that in panel A for the superposed CCHFV N molecules with neighboring CCHFV N molecules in the same helix colored in yellow and CCHFV N molecules in the juxtaposed antiparallel helix colored in black with a semitransparent surface. The arrow indicates the direction of movement. (D) The DEVD cleavage site is exposed when CCHFV N is incubated with primer-length RNA. Purified Ns were treated with or without poly$(U)_{12}$ ssRNA and incubated with human caspase-3. The reaction products were analyzed by SDS-PAGE followed by Western blotting. The pointers show full-length N (56 kDa) and the cleavage product (30 kDa). (E) The amount of cleaved N was measured by densitometry analysis from three independent experiments. The results are expressed as percentages of the cleavage product in reference to total N protein (cleaved and full-length N together).

superhelical polymer and release free, monomeric N (Fig. 4C). By doing so, the bound vRNA would be exposed for transcription or replication to occur. Similarly to the replication cycle of influenza A virus (28, 44), free monomeric CCHFV N might also be essential for viral RNA replication either by interacting with the RNA-dependent RNA polymerase or by binding viral RNAs to prevent degradation.

As we have previously demonstrated, the depletion of CCHFV N by caspase-mediated degradation via the DEVD caspase-3 cleavage site conserved across all strains of CCHFV would be detrimental to the replication cycle of the virus in host cells (21). From the results obtained, it is clear that in the double superhelical polymer, the caspase-3 cleavage site of CCHFV N is obscured and could not be subjected to cleavage by host cell caspase-3. Only

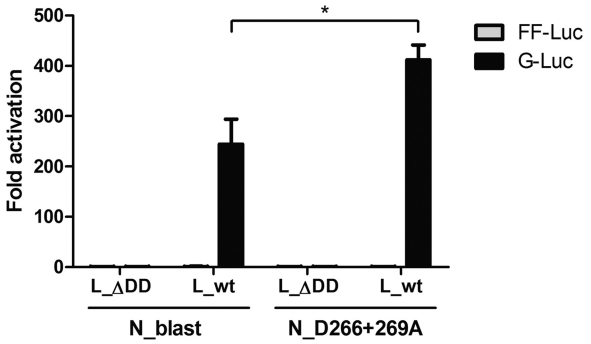

FIG 5 Increase of CCHFV minigenome expression when the caspase recognition site DEVD of CCHFV N is mutated. BSR T7/5 cells were transfected with expression constructs for CCHFV polymerase (wild-type L_wt or inactive L_ΔDD), CCHFV nucleocapsid protein (wild-type N_blast or DEVD mutant N_D266+269A), CCHFV *Gaussia* luciferase minigenome (G-Luc), T7 polymerase, and firefly luciferase (FF-Luc) used as a transfection control. At 48 h after transfection, luciferase activities were determined, and counts were normalized to the negative control in which L_ΔDD is expressed. Mean values of G-Luc (black bars) and FF-Luc (gray bars) and standard errors of the means are shown (assays were triplicates, done twice). Significance is illustrated, with a *t* test *P* value of 0.027 (*).

when free monomeric CCHFV N is released after conformational change upon sensing primer-length RNA would the caspase-3 site be exposed for cleavage. In addition, using a minireplicon system, we were able to demonstrate that mutations of the conserved DEVD site of CCHFV N would enhance the RNA synthesis activity of CCHFV polymerase compared to that of the wild-type CCHFV N.

Interestingly, while the DEVD caspase-3 identification and cleavage site is conserved across different strains of CCHFV, it is not conserved among different species of *Nairovirus* (see Fig. S5 in the supplemental material). As caspase-3 cleavage via this cleavage site reduced CCHFV polymerase transcriptional activity, one may wonder why the site has not been counterselected during the evolution of CCHFV. Further investigation into the replication cycle of the virus and other species of the *Nairovirus* family will be required to determine the importance of the preservation of this cleavage site.

ACKNOWLEDGMENTS

This work was supported by the Small Project Funding 201007176206 of the University of Hong Kong (to M.K.). Y.W. is supported by a postgraduate studentship from the University of Hong Kong. This work is part of the CCH Fever Network (Collaborative Project) supported by the European Commission under the Health Cooperation Work Programme of the 7th Framework Programme (grant agreement no. 260427 to A.M. and F.W.) and is in part supported by Swedish Medical Research Council grant K2010-57X-0349-01-3 (to A.M.).

We are grateful to the staff of beamline 13B1 of the NSRRC, Taiwan, for their help.

REFERENCES

1. **Albertini AA, et al.** 2006. Crystal structure of the rabies virus nucleoprotein-RNA complex. Science **313**:360–363.
2. **Andersson I, et al.** 2004. Role of actin filaments in targeting of Crimean Congo hemorrhagic fever virus nucleocapsid protein to perinuclear regions of mammalian cells. J. Med. Virol. **72**:83–93.
3. **Bergeron E, Albarino CG, Khristova ML, Nichol ST.** 2010. Crimean-Congo hemorrhagic fever virus-encoded ovarian tumor protease activity is dispensable for virus RNA polymerase function. J. Virol. **84**:216–226.
4. **Brunger AT, et al.** 1998. Crystallography & NMR system: a new software suite for macromolecular structure determination. Acta Crystallogr. D Biol. Crystallogr. **54**:905–921.
5. **Brunotte L, et al.** 2011. Structure of the Lassa virus nucleoprotein revealed by X-ray crystallography, small-angle X-ray scattering, and electron microscopy. J. Biol. Chem. **286**:38748–38756.
6. **Carter SD, Barr JN, Edwards TA.** 2012. Expression, purification and crystallization of the Crimean-Congo haemorrhagic fever virus nucleocapsid protein. Acta Crystallogr. Sect. F Struct. Biol. Cryst. Commun. **68**:569–573.
7. **Clerx JP, Casals J, Bishop DH.** 1981. Structural characteristics of nairoviruses (genus Nairovirus, Bunyaviridae). J. Gen. Virol. **55**:165–178.
8. **Emsley P, Cowtan K.** 2004. Coot: model-building tools for molecular graphics. Acta Crystallogr. D Biol. Crystallogr. **60**:2126–2132.
9. **Ergonul O.** 2006. Crimean-Congo haemorrhagic fever. Lancet Infect. Dis. **6**:203–214.
10. **Ferron F, et al.** 2011. The hexamer structure of Rift Valley fever virus nucleoprotein suggests a mechanism for its assembly into ribonucleoprotein complexes. PLoS Pathog. **7**:e1002030. doi:10.1371/journal.ppat.1002030.
11. **Fisher-Hoch SP, et al.** 1995. Crimean Congo-haemorrhagic fever treated with oral ribavirin. Lancet **346**:472–475.
12. **Flick R, Flick K, Feldmann H, Elgh F.** 2003. Reverse genetics for Crimean-Congo hemorrhagic fever virus. J. Virol. **77**:5997–6006.
13. **Green TJ, Zhang X, Wertz GW, Luo M.** 2006. Structure of the vesicular stomatitis virus nucleoprotein-RNA complex. Science **313**:357–360.
14. **Guo Y, et al.** 2012. Crimean-Congo hemorrhagic fever virus nucleoprotein reveals endonuclease activity in bunyaviruses. Proc. Natl. Acad. Sci. U. S. A. **109**:5046–5051.
15. **Hastie KM, Kimberlin CR, Zandonatti MA, MacRae IJ, Saphire EO.** 2011. Structure of the Lassa virus nucleoprotein reveals a dsRNA-specific 3′ to 5′ exonuclease activity essential for immune suppression. Proc. Natl. Acad. Sci. U. S. A. **108**:2396–2401.
16. **Hastie KM, et al.** 2011. Crystal structure of the Lassa virus nucleoprotein-RNA complex reveals a gating mechanism for RNA binding. Proc. Natl. Acad. Sci. U. S. A. **108**:19365–19370.
17. **Hendrickson WA, Horton JR, LeMaster DM.** 1990. Selenomethionyl proteins produced for analysis by multiwavelength anomalous diffraction (MAD): a vehicle for direct determination of three-dimensional structure. EMBO J. **9**:1665–1672.
18. **Iseni F, Barge A, Baudin F, Blondel D, Ruigrok RW.** 1998. Characterization of rabies virus nucleocapsids and recombinant nucleocapsid-like structures. J. Gen. Virol. **79**:2909–2919.
19. **Jin H, Elliott RM.** 1993. Non-viral sequences at the 5′ ends of Dugbe nairovirus S mRNAs. J. Gen. Virol. **74**:2293–2297.
20. **Jones TA, Zou JY, Cowan SW, Kjeldgaard M.** 1991. Improved methods for building protein models in electron density maps and the location of errors in these models. Acta Crystallogr. A **47**:110–119.
21. **Karlberg H, Tan YJ, Mirazimi A.** 2011. Induction of caspase activation and cleavage of the viral nucleocapsid protein in different cell types during Crimean-Congo hemorrhagic fever virus infection. J. Biol. Chem. **286**:3227–3234.
22. **Laskowski RA, MacArthur MW, Moss DS, Thornton JM.** 1993. PROCHECK: a program to check the stereochemical quality of protein structures. J. Appl. Crystallogr. **26**:283–291.
23. **Leblebicioglu H.** 2009. Ribavirin treatment for Crimean-Congo hemorrhagic fever. Jpn. J. Infect. Dis. **62**:485–486.
24. **Maclellan K, Loney C, Yeo RP, Bhella D.** 2007. The 24-angstrom structure of respiratory syncytial virus nucleocapsid protein-RNA decameric rings. J. Virol. **81**:9519–9524.
25. **Mardani M, Jahromi MK, Naieni KH, Zeinali M.** 2003. The efficacy of oral ribavirin in the treatment of Crimean-Congo hemorrhagic fever in Iran. Clin. Infect. Dis. **36**:1613–1618.
26. **McCoy AJ.** 2007. Solving structures of protein complexes by molecular replacement with Phaser. Acta Crystallogr. D Biol. Crystallogr. **63**:32–41.
27. **Morikawa S, Saijo M, Kurane I.** 2007. Recent progress in molecular biology of Crimean-Congo hemorrhagic fever. Comp. Immunol. Microbiol. Infect. Dis. **30**:375–389.
28. **Newcomb LL, et al.** 2009. Interaction of the influenza A virus nucleocapsid protein with the viral RNA polymerase potentiates unprimed viral RNA replication. J. Virol. **83**:29–36.
29. **Noda T, Hagiwara K, Sagara H, Kawaoka Y.** 2010. Characterization of

the Ebola virus nucleoprotein-RNA complex. J. Gen. Virol. **91**:1478–1483.
30. **Osborne JC, Elliott RM.** 2000. RNA binding properties of bunyamwera virus nucleocapsid protein and selective binding to an element in the 5′ terminus of the negative-sense S segment. J. Virol. **74**:9946–9952.
31. **Otwinowski Z, Minor W.** 1996. Processing of X-ray diffraction data collected in oscillation mode. Methods Enzymol. **276**:307–326.
32. **Qi X, et al.** 2010. Cap binding and immune evasion revealed by Lassa nucleoprotein structure. Nature **468**:779–783.
33. **Raymond DD, Piper ME, Gerrard SR, Smith JL.** 2010. Structure of the Rift Valley fever virus nucleocapsid protein reveals another architecture for RNA encapsidation. Proc. Natl. Acad. Sci. U. S. A. **107**:11769–11774.
34. **Richmond KE, Chenault K, Sherwood JL, German TL.** 1998. Characterization of the nucleic acid binding properties of tomato spotted wilt virus nucleocapsid protein. Virology **248**:6–11.
35. **Ruigrok RW, Crepin T, Kolakofsky D.** 2011. Nucleoproteins and nucleocapsids of negative-strand RNA viruses. Curr. Opin. Microbiol. **14**:504–510.
36. **Schneider TR, Sheldrick GM.** 2002. Substructure solution with SHELXD. Acta Crystallogr. D Biol. Crystallogr. **58**:1772–1779.
37. **Schoehn G, et al.** 2004. The 12 A structure of trypsin-treated measles virus N-RNA. J. Mol. Biol. **339**:301–312.
38. **Severson W, et al.** 2005. Essential amino acids of the Hantaan virus N protein in its interaction with RNA. J. Virol. **79**:10032–10039.
39. **Simon M, Falk KI, Lundkvist A, Mirazimi A.** 2006. Exogenous nitric oxide inhibits Crimean Congo hemorrhagic fever virus. Virus Res. **120**:184–190.
40. **Sola M, et al.** 2000. Towards understanding a molecular switch mechanism: thermodynamic and crystallographic studies of the signal transduction protein CheY. J. Mol. Biol. **303**:213–225.
41. **Tawar RG, et al.** 2009. Crystal structure of a nucleocapsid-like nucleoprotein-RNA complex of respiratory syncytial virus. Science **326**:1279–1283.
42. **Terwilliger TC.** 2003. SOLVE and RESOLVE: automated structure solution and density modification. Methods Enzymol. **374**:22–37.
43. **Vorou R, Pierroutsakos IN, Maltezou HC.** 2007. Crimean-Congo hemorrhagic fever. Curr. Opin. Infect. Dis. **20**:495–500.
44. **Vreede FT, Jung TE, Brownlee GG.** 2004. Model suggesting that replication of influenza virus is regulated by stabilization of replicative intermediates. J. Virol. **78**:9568–9572.
45. **Weber F, Mirazimi A.** 2008. Interferon and cytokine responses to Crimean Congo hemorrhagic fever virus; an emerging and neglected viral zonoosis. Cytokine Growth Factor Rev. **19**:395–404.
46. **Whitehouse CA.** 2004. Crimean-Congo hemorrhagic fever. Antiviral Res. **64**:145–160.
47. **Winn MD, Murshudov GN, Papiz MZ.** 2003. Macromolecular TLS refinement in REFMAC at moderate resolutions. Methods Enzymol. **374**:300–321.
48. **Ye Q, Krug RM, Tao YJ.** 2006. The mechanism by which influenza A virus nucleoprotein forms oligomers and binds RNA. Nature **444**:1078–1082.